A microphysiological early metastatic niche on a chip reveals how heterotypic cell interactions and inhibition of integrin subunit β₃ impact breast cancer cell extravasation

Martina Crippa,‡[ab] Simone Bersini,‡[a] Mara Gilardi,‡[cd] Chiara Arrigoni,[a] Sara Gamba,[e] Anna Falanga,[e] Christian Candrian,[af] Gabriele Dubini,[b] Marco Vanoni[g] and Matteo Moretti*[acf]

During metastatic progression multiple players establish competitive mechanisms, whereby cancer cells (CCs) are exposed to both pro- and anti-metastatic stimuli. The early metastatic niche (EMN) is a transient microenvironment which forms in the circulation during CC dissemination. EMN is characterized by the crosstalk among CCs, platelets, leukocytes and endothelial cells (ECs), increasing CC ability to extravasate and colonize secondary tissues. To better understand this complex crosstalk, we designed a human "EMN-on-a-chip" which involves the presence of blood cells as compared to standard metastases-on-chip models, hence providing a microenvironment more similar to the *in vivo* situation. We showed that CC transendothelial migration (TEM) was significantly increased in the presence of neutrophils and platelets in the EMN-on-a-chip compared to CC alone. Moreover, exploiting the EMN-on-chip in combination with multi-culture experiments, we showed that platelets increased the expression of epithelial to mesenchymal transition (EMT) markers in CCs and that the addition of a clinically approved antiplatelet drug (eptifibatide, inhibiting integrin β₃) impaired platelet aggregation and decreased CC expression of EMT markers. Inhibition of integrin β₃ in the co-culture system modulated the activation of the Src-FAK-VE-cadherin signaling axis and partially restored the architecture of inter-endothelial junctions by limiting VE-cadherin[Y658] phosphorylation and its nuclear localization. These observations correlate with the decreased CC TEM observed in the presence of integrin β₃ inhibitor. Our EMN-on-a-chip can be easily implemented for drug repurposing studies and to investigate new candidate molecules counteracting CC extravasation.

[a] Regenerative Medicine Technologies Lab, Ente Ospedaliero Cantonale (EOC), Via Tesserete 46, 6900 Lugano, Switzerland. E-mail: matteo.moretti@eoc.ch

[b] Laboratory of Biological Structures Mechanics, Chemistry, Material and Chemical Engineering Department "Giulio Natta", Politecnico di Milano, Milan, Italy

[c] Cell and Tissue Engineering Laboratory, IRCCS Istituto Ortopedico Galeazzi, Via Galeazzi 4, 20161 Milan, Italy

[d] Institute of Pathology, University Hospital Basel, University of Basel, 4031 Basel, Switzerland

[e] Division of Immunohematology and Transfusion Medicine, Papa Giovanni XXIII Hospital, Bergamo, Italy

[f] Facoltà di Scienze Biomediche, Università della Svizzera Italiana, Via Buffi 13, 6900 Lugano, Switzerland

[g] Dipartimento di Biotecnologie e Bioscienze, Università Milano Bicocca, Piazza dell'Ateneo Nuovo, 1 20126 Milan, Italy

‡ MC, SB and MG contributed equally to this study.

Introduction

Haematogenous metastases develop following a multistep process consisting of many interrelated events, *i.e.* detachment from the primary tumor, intravasation into the vascular system, arrest on the endothelium, extravasation and colonization of distant tissues.[1] A key aspect during the metastatic dissemination is that multiple players establish competitive mechanisms whereby cancer cells (CCs) are exposed to both pro- and anti-metastatic stimuli.[2,3] In particular, during their journey into the circulatory system, CCs simultaneously interact with several blood cell populations, forming the so-called "early metastatic niche" (EMN). A metastatic niche could be defined as a tumor-promoting microenvironment that fosters CC engraftment and proliferation at secondary sites, hence exacerbating the metastatic potential of malignant cells.[4] In particular, the EMN is a specialized microenvironment which develops a few hours after the initial arrest of CCs into the vasculature and

is characterized by the heterotypic crosstalk between granulocytes and aggregates formed by platelets, endothelial cells (ECs) and CCs. The formation of this niche temporally precedes the pro-metastatic interaction between monocytes/macrophages and CCs, and represents a crucial event for the metastatic progression.[5]

Breast cancer preferentially metastasizes to the bone, lungs, regional lymph nodes, liver and brain. Although different metastatic sites seem to have diverse driving signals, the steps preceding the secondary site colonization are shared in the EMN.[5,6] Thus, investigating the interactions occurring in the EMN could provide insights into the mechanisms of metastatic dissemination and then allow to discover potential targets to counteract the early steps of metastasis formation.

Among the components of the EMN, platelets are increasingly being considered as a key player.[7] Platelets have been shown to contribute to the metastatic dissemination through different mechanisms, including the generation of a physical shield around CCs,[8,9] the secretion of factors promoting CC epithelial to mesenchymal transition (EMT),[10,11] the activation of the endothelium[12] and the recruitment of multiple cells fostering the formation of metastases.[13] Furthermore, the depletion of platelets decreased breast cancer derived metastatic foci to the lung and bone in both xenograft and syngeneic tumor models.[14] Beside platelets, several types of immune cells are involved in the metastatic spread: tissue-resident macrophages reach the metastatic niche to support the metastasis while the interaction between granulocytes and CCs has been reported to assist CC spread, hence promoting their arrest and extravasation.[5] In this scenario, neutrophils play a controversial role. Tumor-entrained neutrophils were reported to inhibit the metastatic seeding of CCs[2] and blockade of specific signaling pathways in the tumor microenvironment was associated with the presence of cytotoxic neutrophils.[15] However, other studies either demonstrated that neutrophil depletion did not influence the number of metastatic foci[16] or that neutrophils positively regulated the formation of metastases.[17-20] In this scenario, recent studies highlighted that neutrophils enable circulating tumor cells lodging at the metastatic site[21] and also contribute to increasing the extravasation potential of adjacent tumor cells through modulation of the endothelial barrier.[22] Overall, these conflicting results highlight a heterogeneous body of literature and allow to suggest that context-dependent stimuli from the local microenvironment could influence the phenotype and behavior of neutrophils and other immune cells.[23] Interestingly, it was suggested that the tumoricidal interaction between CCs and neutrophils only occurs in the pre-metastatic tissue but not at the primary site.[24]

No current model can fully elucidate the complex and reciprocal interactions occurring in the EMN. *In vivo* animal models could be biased by differences existing between mouse and human immune systems, which have not been entirely overcome by humanized mouse models.[25] Furthermore, *in vivo* studies do not allow to easily isolate specific cell–cell interactions within complex environments. On the other side, standard *in vitro* models (*e.g.* commercial Boyden chamber for cell migration and invasion assays[26]) can overcome this limitation, although these assays lack the physiological 3D architecture and functionality characterizing *in vivo* tissues. In this scenario, microfluidic[27] and mesoscale systems[28] have shown the possibility to couple the analytical advantages of traditional 2D *in vitro* assays with a more reliable modeling of the *in vivo* tissue microarchitecture and its biochemical milieu. Microfluidic systems are increasingly being used especially in the context of cancer metastasis formation because they allow to focus on the interaction of CCs with immune cells, such as neutrophils,[22,29] and with the endothelium, hence replicating the microvasculature microenvironment.[22,29,30] Relevant advantages of these models are the possibility to easily visualize and spatio-temporally control specific biological processes, including cellular transendothelial migration (TEM) or extravasation.[22,29,30] Microfluidic models were also exploited to test the effect of specific drugs in preventing platelet extravasation.[30]

In this work, we describe the generation of a vascularized 3D microenvironment which allows the perfusion of CCs, platelets and neutrophils to replicate key features of the EMN (*i.e.* EMN-on-a-chip). In parallel, we setup multi-culture experiments to partially elucidate the complex interactions occurring in the EMN and to characterize the effects of integrin β_3 inhibition. We focused on breast cancer using the MDA-MB-231 triple negative breast CC line, which is recognized for its high metastatic potential. Noteworthy, metastatic breast CC lines have been already used *in vivo* for EMN studies.[3]

Inhibition of specific components of the EMN can be achieved by targeting their receptors or signaling proteins. Drugs blocking COX (*e.g.* aspirin), ADP receptor P2Y12 (*e.g.* clopidogrel) and integrin β_3 (*e.g.* eptifibatide) are widely used to target platelets and treat cardiovascular diseases which are not associated with cancer, such as coronary syndrome.[31,32] Some of these drugs have demonstrated anti-metastatic effects,[33,34] although their mechanisms of action are not yet fully understood. Indeed, it is possible that the anti-neoplastic properties shown by these therapeutics could be related to their effects on multiple cell types of the tumor microenvironment,[35] which have never been fully analyzed in a 3D microenvironment. Among the available anti-platelet drugs, eptifibatide (integrin β_3 inhibitor) was chosen because it is already clinically approved as anti-aggregant for the treatment of patients with cardiovascular diseases. Furthermore, in a mouse model eptifibatide was shown to preserve platelet functionality in haemostasis while inhibiting CC induced platelet aggregation.[36] For all these reasons, eptifibatide could represent a platelet-modulating therapeutic that can be used to impair the formation of breast cancer metastases.

Here we demonstrate that eptifibatide, besides limiting platelet activation and aggregation, impairs CC extravasation by acting on both CC themselves and the endothelium. The strategy here presented allowed us to dissect some of the key heterotypic interactions occurring among the different components of the EMN and to better characterize the previously neglected effects of a clinically approved drug.

Materials and methods

Generation of the "early metastatic niche-on-a-chip"

A silicon wafer with the desired geometry was produced through standard soft lithography techniques, then poly-dimethyl-siloxane (PDMS, Sylgard) was poured on the wafer and cured in an oven at 80 C for 2 h. Once polymerized, the PDMS was removed from the wafer, inlets/outlets were created with biopsy punches (4 mm biopsy punch for the media channels and 1 mm biopsy punch for the gel channels) and the PDMS was attached to a glass coverslip through plasma bonding. The obtained microfluidic chip consisted of three hydrogel regions each flanked by two lateral media channels (Fig. 1A and B), separated by trapezoidal posts to allow the confinement of the hydrogel matrix, as we already reported.[37]

Following microfabrication and sterilization of the microfluidic chip, we generated microvascularized 3D environments inside the central hydrogel region (Fig. 1A). Green fluorescent protein (GFP)-transfected human umbilical vein endothelial cells (HUVECs, Angioproteomie) were resuspended at a density of 3.5×10^6 cells per ml in a solution of endothelial growth medium (EGM)-2 (Lonza) medium with 5% FBS (Fisher Scientific) containing 4 IU ml^{-1} thrombin (Baxter) to promote fibrinogen polymerization and form a stable fibrin matrix. The cell suspension was then 1 : 1 mixed with a 5 mg ml^{-1} fibrinogen (Sigma) solution and injected in the central hydrogel channel. The two lateral hydrogel channels were seeded with a 4×10^6 cells per ml suspension of lung fibroblasts (Lonza). Briefly, lung fibroblasts were resuspended in EGM-2 medium with 5% FBS containing 4 IU ml^{-1} thrombin and then 1 : 1 mixed with a 5 mg ml^{-1} fibrinogen solution and injected in the channels. Lung fibroblasts were added in the chip with the sole purpose to promote vessel formation through the continuous secretion of paracrine factors (Fig. 1A).[38] The presence of fibroblasts in the model is fundamental to promote the formation of a branched and interconnected network of perfusable vessels. After 20 min gelation, the media channels were filled with EGM-2. The medium was replenished every day until the fourth day of culture when mature and perfusable vascular networks were formed.

Vessel permeability was quantified by injecting 10 μl 70 kDa TRITC Dextran (2.5 mg ml^{-1}, Chondrex) in one of the media channels adjacent to the vascular network channel. Six regions of interest (ROIs) (40 μm × 20 μm) for each device were analyzed when injecting dextran ($t = 0$) and after 1 minute. Permeability was quantified in terms of increase of
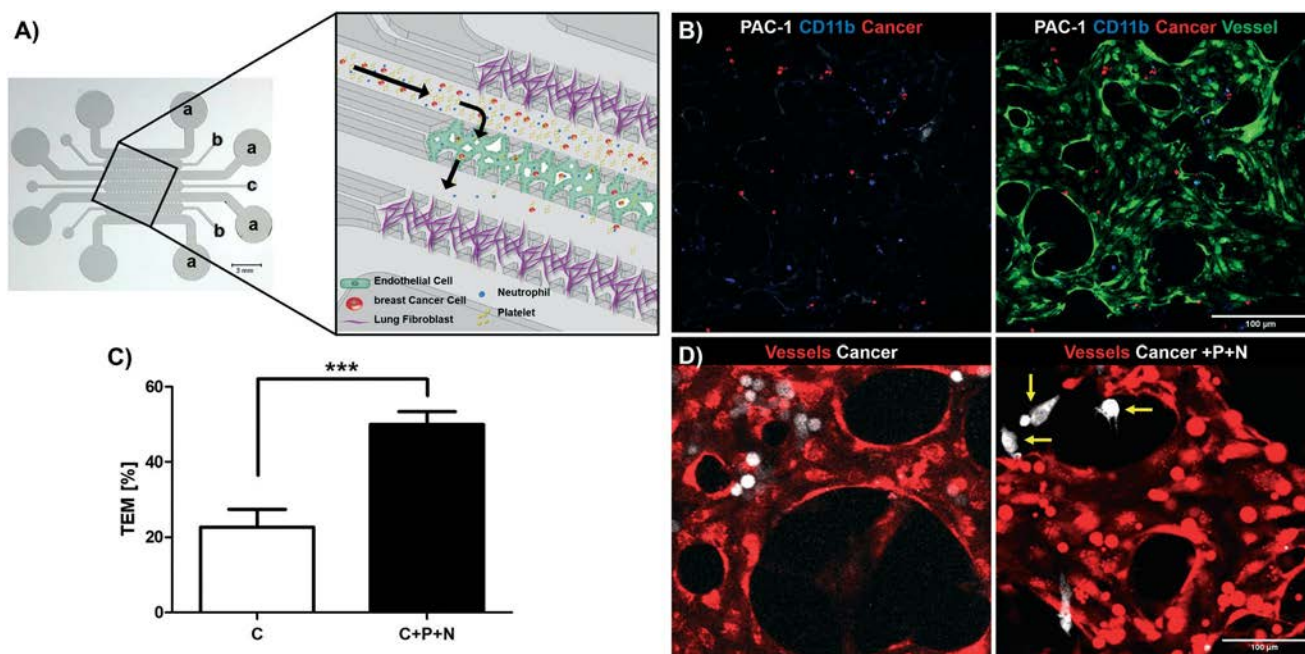

Fig. 1 CC extravasation in presence of platelets and neutrophils in the EMN in 3D microfluidic models of human microvasculature. Microfluidic device, schematics of the chip channels (A): media channels (a), lung fibroblast channels (b), microvascular network channel (c). Live imaging capturing each component of the EMN (B): platelets (PAC-1, white), neutrophils (CD-11b, blue), CCs (red) and vessels (green). CC TEM (at least $n = 6$, ***: $p = 0.0004$) (C). TEM of CCs alone and in presence of platelets and neutrophils. CCs are white and vessels are red. Extravasated CCs are pointed with yellow arrows. Platelets and neutrophils are not stained (D). All fluorescence images were taken with an original 4× magnification. Legend: C (cancer), P (platelets), N (neutrophils).

fluorescence intensity in the matrix region surrounding each vessel between the two-time steps. Data were normalized to the initial fluorescence intensity ($t = 0$).[39]

Platelets and neutrophils were isolated from commercially available human buffy coats the day before seeding into microfluidic devices. A preliminary centrifugation step with Ficoll (Sigma) gradient allowed to separate blood components according to their molecular weight, then platelets were harvested, purified with Krebs ringer solution washings and finally precipitated with centrifugations (10 min at 3500 rpm). Neutrophils were isolated from the same Ficoll solution, incubated for 1 h in 3% dextran T500 (Pharmacosmos) and purified from red blood cells with Red Blood Cell Lysis Solution (Miltenyi). Isolated platelets and neutrophils were suspended in EGM-2 at physiological densities (200×10^6 cells per ml and 3.5×10^6 cells per ml, respectively) and seeded on top of monolayers of red fluorescent protein (RFP)-transfected MDA-MB-231 (Angioproteomie) breast CCs, which were previously set up in traditional culture dishes. Cells were kept in culture for 24 h with or without the addition of eptifibatide (15 μg ml^{-1} final concentration from a stock of commercially available Integrilin (2 mg ml^{-1} liquid solution)). In the meantime, microfluidic devices were pre-treated with EGM-2 medium containing 15 μg ml^{-1} eptifibatide. The day after, cells were detached from the culture dishes and a volume of 50 μl containing CCs (400 000 cells per ml), platelets and neutrophils was injected in one of the two medium channels adjacent to the central hydrogel channel containing microvascular networks. The seeding of CCs, platelets and neutrophils was performed under passive flow conditions (generated by injecting the above-mentioned volume in the medium channel). The pressure drop then decreased over time, hence determining a decrease in the velocity of CCs flowing through the channel and the microvascular network. After a few minutes, the flow spontaneously stopped, therefore CC adhesion and TEM analyses were performed under static conditions.

For 2D co-culture experiments, monolayers of ECs (alone or in co-culture with CCs) were prepared the day before the isolation of blood components. Platelets (200×10^6 cells per ml) and neutrophils (3.5×10^6 cells per ml) were suspended in EGM-2 as previously described and incubated with ECs and/or CCs for 24 h with or without the addition of eptifibatide (15 μg ml^{-1}). To avoid any alteration of platelet activation/aggregation, EGM-2 containing heat-inactivated serum and without heparin was used in all the experiments.

Evaluation of CC adhesion, TEM and invasion

To analyze CC adhesion and TEM, microfluidic chips were fixed with 2% paraformaldehyde (PFA, Millian) at 2 h and 5 h after CC injection, respectively, and subsequently imaged under a confocal microscope. Stacks of 50 μm height were acquired for both TEM and adhesion analyses. For TEM, at least 3 ROIs per chip of 1.2 mm × 1.2 mm including both

microvascular networks and extracellular matrix were analyzed. We analyzed superimposed images of CCs (RFP) and ECs (GFP) channels and through the stacks obtained by confocal microscope we were able to visualize the spatial position of CCs compared to the endothelial network. Only those CCs that were located completely outside the network were considered as transmigrated cells. The TEM rate was obtained by dividing the number of completely transmigrated CCs by the total number of CCs in each ROI. To analyze CC adhesion inside microvascular networks three ROIs of 680 μm × 680 μm per device were randomly acquired along the network channel, including both microvascular networks and extracellular matrix. The adhesion rate was quantified by normalizing the number of adherent CCs of each ROI to the area covered by the network in each specific ROI.

The invasiveness of CCs was tested in a microfluidic chip including an acellular fibrin gel channel. The suspension of CCs (4×10^6 cells per ml), platelets (200×10^6 cells per ml) and neutrophils (3.5×10^6 cells per ml) in EGM-2 was injected in one of the medium channels adjacent to the fibrin gel, while in the other medium channel we introduced EGM-2 supplemented with basic fibroblast growth factor (b-FGF) (50 ng ml^{-1}; Peprotech) and vascular endothelial growth factor (VEGF) (50 ng ml^{-1}; Peprotech) to create a chemoattractant gradient and promote CC invasion.[40] The microfluidic chips were fixed 24 h after cell seeding. CC invasion was quantified by counting the number of invaded CCs into the fibrin gel in three random ROIs of 480 μm × 350 μm per device including both fibrin gel and media channel.

Immunofluorescence analyses and live imaging

Co-cultures were fixed with 2% PFA for 10 min, treated with 0.1% Triton X-100% (Sigma) for 10 min and incubated with 5% bovine serum albumin (ThermoFisher Scientific) for 1 h at RT. Primary antibodies were incubated for 2 h at RT. After washing in PBS (ThermoFisher Scientific), samples were incubated with secondary antibody for 1 h at RT. The following primary antibodies were used: plasminogen activator inhibitor (PAI, Santa Cruz Biotechnology; dil. 1 : 100), matrix metalloprotease (MMP)-9 (SantaCruz Biotechnology; dil. 1 : 100), integrin $\alpha_{IIb}\beta_3$ (Santa Cruz Biotechnology; dil. 1 : 100), PAC-1 (Santa Cruz Biotechnology; dil. 1 : 100), CD11b (Biolegend; dil. 1 : 100), vascular endothelial (VE)-cadherin (Cell Signaling; dil. 1 : 100) and phospho VE-cadherin Y658 (ThermoFisher Scientific; dil. 1 : 100), focal adhesion kinase (FAK) and phospho FAK Y397 (ThermoFisher Scientific; dil. 1 : 100), proto-oncogene tyrosine-protein kinase Src and phospo Src Y416 (Cells Signaling; dil. 1 : 100). Antibody dilutions were set accordingly to the manufacturer recommendations. Images were acquired with a Nikon confocal microscope and processed with ImageJ software for morphological analyses. For live imaging within microfluidic chips, platelets and neutrophils were stained immediately after blood component isolation. Platelets were incubated with antibody against PAC-1 for 45 min at RT, while neutrophils were stained with anti-CD11b for 30 min at RT.

Western blot

ECs and CCs were co-cultured for 2 days and then sorted through the following protocol. The medium containing platelets and neutrophils in suspension was aspirated from each well. Cocultures were then washed with warm PBS and then incubated with trypsin for 3 min. Cells were then immediately incubated in DMEM supplemented with 10% FBS to block trypsin. Cells were centrifuged and incubated in PBS containing 0.1% BSA, 2 mM EDTA and 5 µg ml^{-1} biotinylated anti-human CD31 (eBioscience) to specifically label endothelial cells for 10 min at 4 C under gentle stirring. After washing in PBS containing 0.1% BSA and 2 mM EDTA, cells were centrifuged and then incubated in the same buffer containing streptavidin-coated magnetic beads (25 µl from the CELLection biotin binder kit according to the manufacturer instructions, ThermoFisher Scientific) for 20 min at 4 C under gentle stirring. Endothelial cells were finally separated from CCs and any potential residue of other cell populations by using DynaMag-2 magnet (ThermoFisher Scientific). The cells were then lysed in RIPA buffer (ThermoFisher Scientific) supplemented with a protease inhibitor cocktail and 1 mM phenylmethylsulfonyl fluoride (PMSF, Sigma-Aldrich) for 30 min on ice, then centrifuged at 14 000 rpm for 10 min at 4 C and stored at −20 C. Protein content was determined with Pierce BCA protein assay (ThermoFisher Scientific). Proteins (60 µg) were loaded on 8% sodium dodecyl sulfate (SDS)-polyacrylamide gels and then electroblotted onto Hybond-P polyvinylidene difluoride transfer membranes (BioRad Laboratories). After blocking (5% BSA, 4 C, overnight), the membranes were incubated overnight at 4 C with the following primary antibodies, according to the manufacturer instructions: glyceraldehyde-3-phosphate dehydrogenase (GAPDH), PAI (Santa Cruz Biotechnology; dil. 1 : 200), (MMP)-9 (Santa Cruz Biotechnology; dil. 1 : 200), focal adhesion kinase (FAK) (total and phosphorylated) (ThermoFisher Scientific; dil. 1 : 100), extracellular signal-regulated kinase (ERK) (total and phosphorylated) (ThermoFisher Scientific; dil. 1 : 1000), protein kinase B (AKT) (total and phosphorylated) (Santa Cruz Biotechnology; dil. 1 : 200), cyclin-dependent kinase (CDK)-5 (Santa Cruz Biotechnology; dil. 1 : 200), TALIN-1 (TLN1, total and phosphorylated) (Abcam; dil. 1 : 100), proto-oncogene tyrosine-protein kinase Src (total and phosphorylated) (Cells Signaling; dil. 1 : 100), VE-cadherin (total (Cell Signaling; dil. 1 : 1000) and phosphorylated (ThermoFisher Scientific; dil. 1 : 1000)), integrin $\alpha_{IIb}\beta_3$ (Cell Signaling; dil. 1 : 1000). Obtained data were quantified with ImageJ (Analyze − Gel). Each protein expression was normalized to the relative GAPDH. When we examined the expression of both the phosphorylated and the total form of a protein, we presented the data as the ratio of these two values. Data were normalized to the expression level in non-treated (*i.e.* no drug) samples.

Statistics

Statistical differences between experimental groups were quantified through Student's *t*-test, unless specified in the figure legend (Prism, Graph Pad). Differences were considered significant for $p < 0.05$ (*), $p < 0.01$ (**) and $p < 0.001$ (***). Results were presented as mean ± standard error of the mean (SEM). Details on number of biological replicates (*n*), exact *p*-values and data normalization are reported in each figure legend.

Results

A matter of 4 players: characterizing the heterotypic interactions occurring in the early metastatic niche

To comprehensively analyze the interactions occurring in the complex microenvironment of the EMN we combined 3D microphysiological systems and classical 2D assays, that we exploited as a preliminary test to study the interactions between each component of the niche.

Platelets and neutrophils isolated from whole blood were positively stained for cell identity markers (ESI† Fig. S1A, PAC-1 for activated platelets and CD11b for activated neutrophils). We then verified platelet activation in the co-culture system through the quantification of P-selectin surface expression. Platelets were incubated with or without CCs and ECs in EGM-2. The presence of EGM-2 slightly increased the expression of P-selectin after 24 h, as compared to the basal level of P-selectin detected in fresh platelets[41] (8.8% *vs.* 0.5%) (ESI† Fig. S1B and C). However, platelet activation was significantly enhanced by the addition of CCs in all tested time points ($p < 0.001$). At 24 h incubation, the average platelet P-selectin expression was 16.3% with CCs as compared to 8.8% in EGM-2 medium ($p < 0.001$) and was further increased in presence of both CCs and ECs, reaching 31% ($p < 0.001$ as compared to both CCs and EGM-2) (ESI† Fig. S1B and C).

Next, we determined the effects of platelets, neutrophils and ECs on the phenotype of CCs by investigating morphological changes in terms of major/minor axis ratio and circularity index (ESI† Fig. S2A). In control conditions CCs elongated on the culture substrate,[42-44] while we found that addition of neutrophils (C + N) induced CCs to assume a more rounded shape compared to all the other co-culture conditions (ESI† Fig. S2B and C). This rounded morphology was not due to CC death, as shown by negative DRAQ7 staining of CCs (ESI† Fig. S2E). Similar trends in terms of major/minor axis ratio and circularity were quantified when CCs and neutrophils were co-cultured with platelets (C + N + P), while the simultaneous presence of ECs partially reversed the effect (ESI† Fig. S2B and C).

Finally, we analyzed the effects of CCs, platelets and neutrophils on the endothelium (ESI† Fig. S2D). The addition of CCs decreased the surface covered by ECs compared to control conditions with ECs only ($39.26 \pm 3.21\%$ *vs.* $44.68 \pm 3.60\%$), although there was no statistical difference. On the other hand, the presence of platelets increased the area covered by ECs in presence of CCs from $39.26 \pm 3.21\%$ (ECs + CCs) to $55.19 \pm 1.71\%$ (ECs + CCs + P, $p < 0.05$). This effect was further increased by the additional presence of

neutrophils, bringing the percentage of the area covered by ECs from $44.68 \pm 3.60\%$ (ECs) and $39.26 \pm 3.21\%$ (ECs + CCs) to $60.05 \pm 2.40\%$ ($p < 0.05$ and $p < 0.01$, respectively).

CC extravasation in the "EMN-on-a-chip"

Perfusable 3D microvascular networks were generated within microfluidic devices (Fig. 1A), which were imaged for typical markers of activated platelets and neutrophils (PAC-1 and CD11b, respectively, Fig. 1B), showing the presence of functional components of the EMN. Right after the injection, the suspension of CCs, platelets and neutrophils flowed through the microvascular network and CCs either slowed down and arrested on the endothelium or remained trapped within small vessels (Fig. 1D), and finally extravasated mimicking the TEM process observed in the EMN. ESI† Video

S1 shows the suspension of CCs, neutrophils and platelets flow into the microvascular network right after their injection.

This behavior finely recapitulates the process of CC adhesion and TEM occurring in post-capillary venules *in vivo*. Image analysis showed that CC TEM rates were significantly higher for CCs with platelets and neutrophils compared to CCs alone (49.99 ± 3.39 *vs.* 22.66 ± 4.75, $p < 0.001$) (Fig. 1C).

Eptifibatide decreases CC TEM and impairs platelet aggregation and activation

We then exploited the combination between the microfluidic model (*i.e.* EMN-on-a-chip) and the related multi-culture systems to evaluate the outcome of the clinically approved β_3 inhibitor eptifibatide on CC extravasation (EMN-on-a-chip)
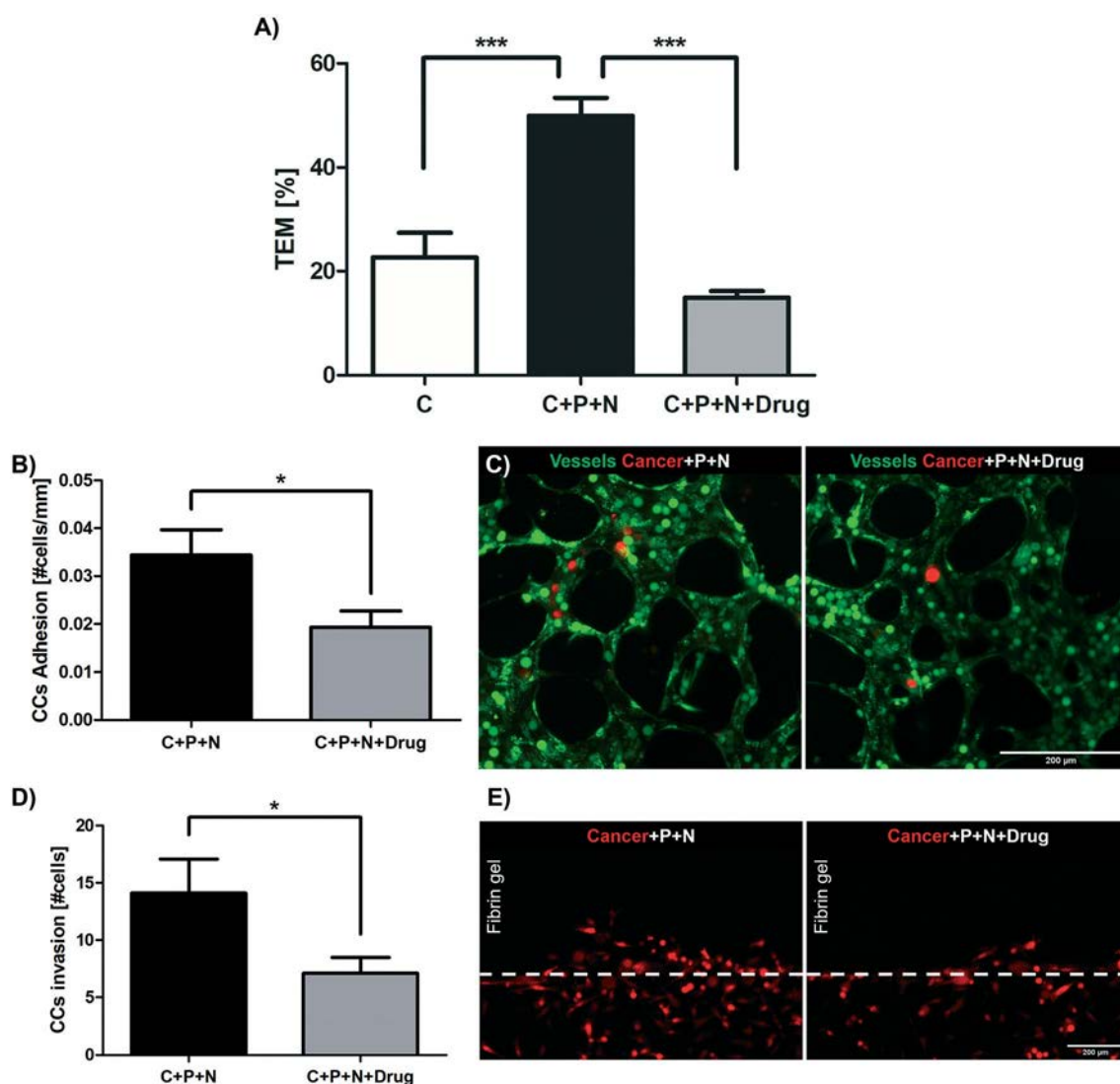

Fig. 2 Eptifibatide affects each step of CC TEM and microvascular network development. Quantification of TEM (at least $n = 6$, ***: $p < 0.001$; *: $p < 0.05$) (A), vascular adhesion ($n = 24$ in 6 biological replicates, $p = 0.0212$ for C + P + N *vs.* C + P + N + drug) (B and C). Quantification of CC invasion ($n = 18$, *: $p = 0.0391$ for C + P + N *vs.* C + P + N + drug) (D and E). All fluorescence images were taken with an original 10× magnification. Legend: C (cancer), P (platelets), N (neutrophils).

and to dissect its effects on each component of the EMN (3D and 2D multi-culture systems). Pre-incubating CCs with platelets and neutrophils in presence of the β_3 inhibitor significantly impaired TEM in the EMN-on-a-chip, as compared to untreated samples (14.99 ± 1.26% *vs.* 49.99 ± 3.39%, $p < 0.001$) (Fig. 2A).

Moreover, TEM values were even lower compared to the ones quantified with CCs alone (14.99 ± 1.26% *vs.* 22.66 ± 4.75%, $p < 0.05$). The higher extravasation rate detected in presence of platelets and neutrophils compared to CCs alone confirmed the critical role that the immune system plays in this step of the metastatic process.[5,7] The decrease of CC TEM with the inhibition of integrin β_3 was related to the decreased adhesion of CCs to the endothelium and lowered CC invasiveness of a 3D matrix. Indeed, eptifibatide reduced CC adhesion to the vascular network in presence of neutrophils and platelets, in terms of number of adherent CCs normalized to the area of the network (0.019 ± 0.003 *vs.* 0.034 ± 0.005, $p < 0.05$) (Fig. 2B and C). The addition of the drug to the suspension of platelets, neutrophils and CCs significantly reduced also the ability of CCs to invade a 3D matrix under chemotactic stimuli (50 ng ml^{-1} b-FGF and 50 ng ml^{-1} VEGF) (7.11 ± 1.38 *vs.* 14.11 ± 2.96, #cells) (Fig. 2D and E).
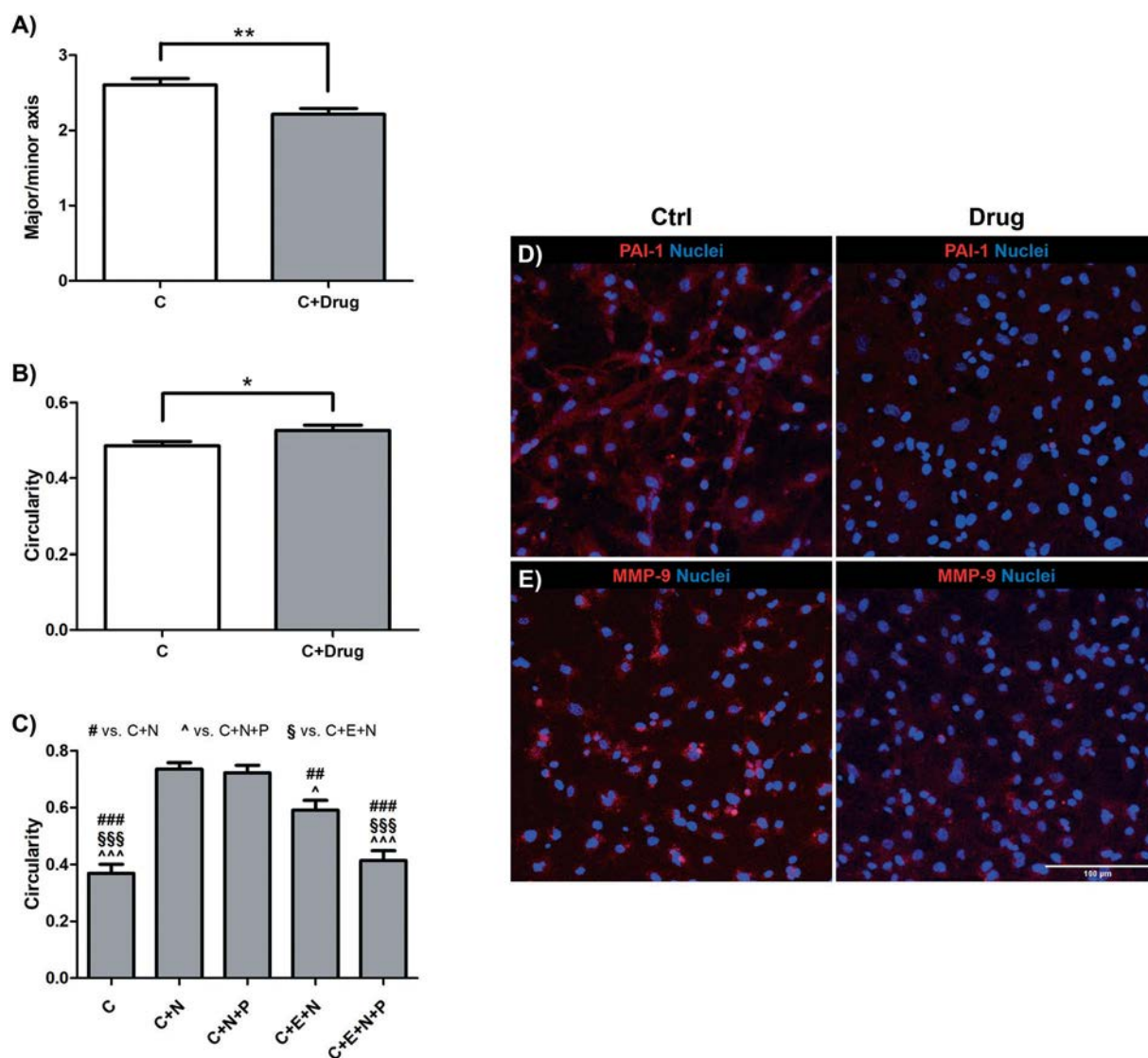

Fig. 3 Eptifibatide affects CC morphology and reduces the expression of CC invasive markers. Effect of the drug on CC major/minor axis (2.22 ± 0.08 *vs.* 2.60 ± 0.09; $p = 0.0011$) (A) and circularity (0.53 ± 0.01 *vs.* 0.49 ± 0.01; $p = 0.0263$) (B). A and B: Aggregate result considering all the potential combinations of co-culture. Effect of eptifibatide on CC circularity in specific co-culture conditions including neutrophils (at least $n = 27$ measurements in 3 biological replicates, #: $p < 0.05$ compared to the group cancer cells + neutrophils (C + N); ^: $p < 0.05$ compared to the group cancer cells + neutrophils + platelets (C + P + N); §: $p < 0.05$ compared to the group cancer cells + endothelial cells + neutrophils (C + E + N)) (C). Immunofluorescence image of two representative CC invasive markers, *i.e.* PAI-1 (D) and MMP-9 (E). Markers: red; nuclei: blue. All fluorescence images were taken with an original 4× magnification and then magnified 4×. Legend: C (cancer), P (platelets), N (neutrophils), E (endothelial cells). Statistical differences in Fig. 3C were quantified using ANOVA test with Bonferroni correction.

Finally, addition of the integrin β_3 inhibitor not only decreased the activation of $\alpha_{IIb}\beta_3$ on platelets co-cultured with CCs, ECs and neutrophils, as expected (shown by decreased staining for PAC-1, marker of $\alpha_{IIb}\beta_3$ activation) (ESI† Fig. S3A), but also reduced its expression (ESI† Fig. S3B).

Eptifibatide decreases the expression of invasion markers in CCs

To check if the effects of eptifibatide on CC TEM, adhesion and invasion were caused by a direct effect on CCs, we added integrin β_3 inhibitor to co-cultures, showing a significantly
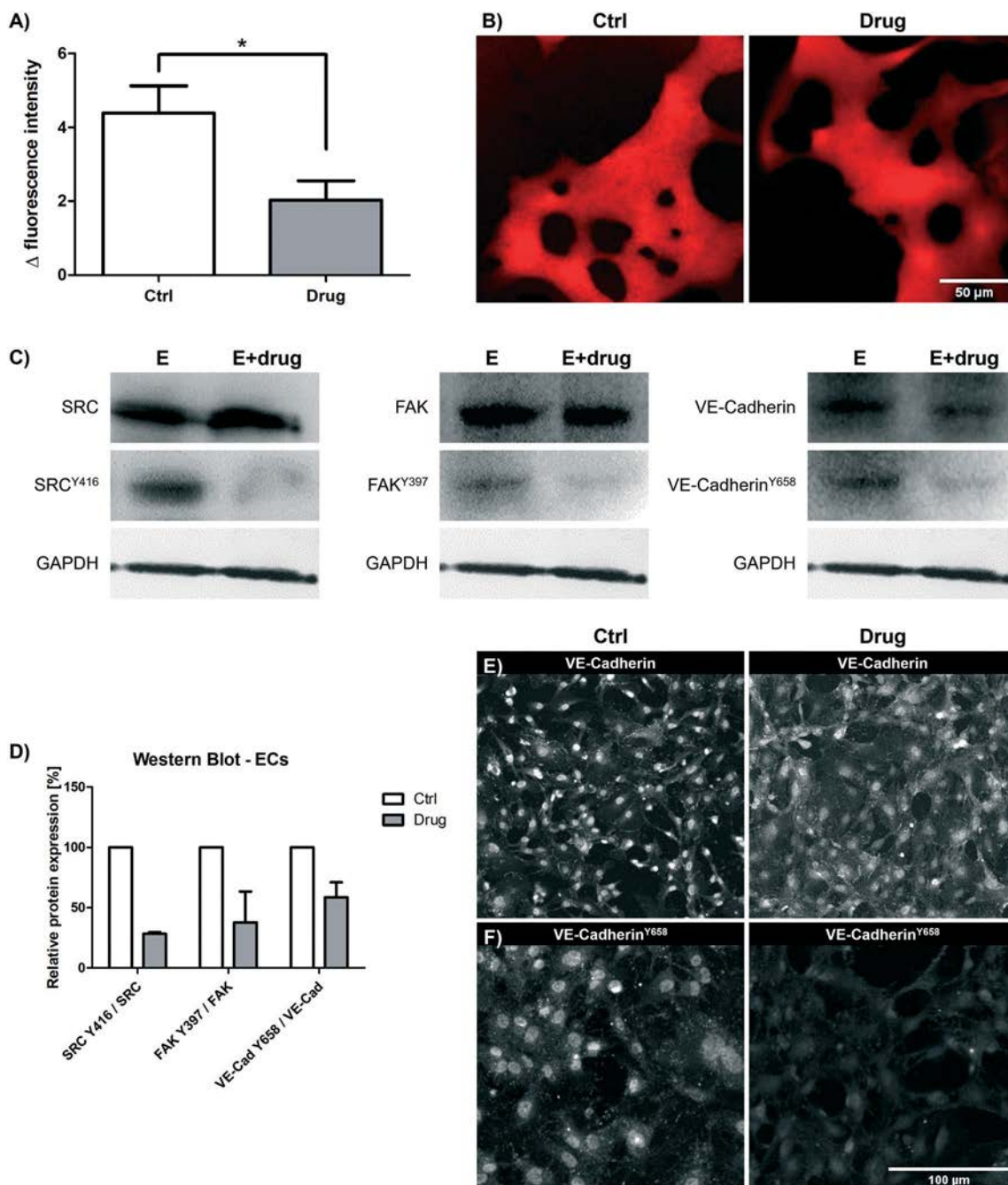

Fig. 4 Eptifibatide decreases microvessel permeability partially restoring the architecture of inter-endothelial junctions. The increment of fluorescence intensity of 70 kDa TRITC dextran (red) was significantly lower in the microvasculature treated with eptifibatide ($n = 10$ in 3 biological replicates; $p = 0.033$) (A). Fluorescence images of 70 kDa dextran flowing into microvessel were taken with a 10× original magnification and then magnified 4 times (B). Western blot of key proteins involved in the regulation of the stability of adherens junctions (C). Quantification of Western Blot data on ECs. Data reported are normalized to GAPDH. The data show the percentage of protein expression of drug treated samples compared to non-treated samples, which are arbitrarily normalized to 100% ($n = 2$ replicates) (D). Immunofluorescence staining of VE-cadherin and VE-cadherin Y658 (white) w/ and w/o eptifibatide (E and F). ECs were sorted from co-culture conditions with CCs, neutrophils and platelets. Immunofluorescence images were taken with an original 10× magnification.

reduced CC elongation in all experimental conditions, both in terms of decreased major/minor axis ratio (2.6 ± 0.09 *vs.* 2.22 ± 0.08, $p < 0.001$) and of increased circularity index (0.49 ± 0.01 *vs.* 0.53 ± 0.01, $p < 0.05$) (Fig. 3A−C).

To further confirm the effect of integrin β_3 inhibition on CCs, we investigated the expression of key proteins involved in cancer EMT. Immunofluorescence staining of co-cultures containing CCs, ECs, platelets and neutrophils suggested that integrin β_3 inhibition reduced the expression of two key markers of cancer EMT, *i.e.* PAI-1 (Fig. 3D) and MMP-9 (Fig. 3E). Viable CCs were then sorted from co-cultures with ECs, platelets and neutrophils, and analyzed through Western blot looking for specific proteins involved in invasion and focal adhesion formation/remodeling/activation. To support our claim, Western Blot results suggested that treatment with eptifibatide decreases CC expression of Talin-1 (TLN1) and its phosphorylated form $TLN1^{S425}$, focal adhesion kinase $(FAK)^{Y397}$ and cyclin dependent kinase (CDK)-5 (ESI† Fig. S4A and C). In addition, we found a modest decrease in the expression of AKT and ERK, two key proteins involved in cell proliferation and malignant cell growth (ESI† Fig. S4B and C).[45]

Eptifibatide affects EC permeability altering the activation and localization of cell adhesion molecules

The endothelium expresses integrin $a_V\beta_3$ (ref. 46) and eptifibatide is known to inhibit this dimeric form[47] in addition to inhibiting $\alpha_{IIb}\beta_3$ (mainly expressed by platelets). We thus verified the effect of the inhibitor on ECs in terms of microvessel permeability comparing EGM-2 with or without integrin β_3 inhibitor. We found that the addition of the drug significantly reduced vascular permeability (2.030 ± 0.524 *vs.* 4.388 ± 0.737; $p < 0.05$) (Fig. 4A and B). We then compared microvessel formation with and w/o the integrin β_3 inhibitor in order to check if eptifibatide could have compromised signaling pathways involved in vasculogenesis. We found that the total length of microvascular networks was statistically different comparing control microvascular networks and vessels treated with eptifibatide (2473 ± 71.39 *vs.* 3193 ± 210.4, $p < 0.05$) (ESI† Fig. S5A). We also set co-cultures of ECs with all the components of the niche and we observed that the addition of the drug did not alter the EC area fraction trend observed in absence of Eptifibatide (ESI† Fig. S5B).

We then sorted viable ECs from co-cultures and performed Western Blot analyses. Collected data suggest that treatment with eptifibatide reduced Src^{Y416}, FAK^{Y397} and VE-Cadherin^{Y658} in ECs (Fig. 4C and D). To confirm these results in 3D conditions, we performed immunofluorescent staining of the microvasculature developed on-chip and we observed the same reduction of FAK^{Y397}, Src^{Y416} and VE-cadherin^{Y658} expression in networks treated with eptifibatide. At the same time the total expression of FAK and VE-cadherin did not seem to be affected by the addition of the drug (ESI† Fig. S6). Finally, treatment with eptifibatide partially restored the localization of VE-cadherin at cell boundaries (Fig. 4E) and decreased the nuclear translocation of phosphorylated VE-cadherin (Fig. 4F).

Discussion

In this work we designed a novel microenvironment (*i.e.* the EMN-on-a-chip), based on our previously developed model,[37] which allowed us to mimic the EMN, analyze the contribution of immune cells on CC extravasation and test the effect of an already clinically approved anti-aggregant drug. Combining the EMN-on-a-chip with traditional multi-culture experiments we were able to analyze some of the reciprocal and dynamic interactions occurring between CCs (MDA-MB-231 breast CCs), ECs (HUVECs) and blood cells in the context of breast cancer metastases. Firstly, we designed a large number of preliminary co-culture experiments to quantify macroscopic changes in terms of CC morphology, platelet aggregation and EC coverage of 2D substrates. Then, we analyzed functional changes of both CCs (*e.g.* adhesion, TEM, invasion) and ECs (*e.g.* vascular permeability, vascular branching) in a more physiological-like 3D microenvironment. Within the EMN, platelets and neutrophils enhanced the invasive ability of CCs leading to increased TEM. At the same time, the interplay with CCs and the contact with the endothelium altered the activation state of platelets and immune cells, hence generating a dynamic microenvironment where unique cell−cell interactions drive the metastatic spread.[12,48]

Previous *in vivo* and *in vitro* studies demonstrated that platelets increase CC early metastatization.[10] On the other side, the role of neutrophils is still controversial. Indeed, several works described a pro-tumor effect of neutrophils[49] and other immune cells.[5,17,20,50] However, other studies pointed out a potent anti-tumor activity of neutrophils.[2,15] Our data on CC morphological changes suggest a potential anti-tumor effect of neutrophils coupled with a pro-tumor role of platelets. In particular, our multi-culture experiments suggest that the presence of neutrophils shifted CCs towards a less aggressive phenotype, although more proteomic data and functional assays are required to confirm this finding. This effect was reduced in presence of platelets and ECs, highlighting that either the particular niche composed by platelets and ECs affects the behavior of neutrophils or that the pro-tumor effects of platelets partially mask the anti-tumor role of neutrophils.

Interactions among the components of the EMN also induced significant changes to EC shape and organization. The endothelium represents a key component of the EMN, mediating both CC extravasation[36,51] and survival/dormancy of disseminated CCs.[52] Here we showed that the presence of CCs reduced the area covered by ECs, in agreement with other studies demonstrating that CCs secrete molecules[53] which impair both structure and function of the endothelium.[54] However, addition of platelets, neutrophils or both to CCs + ECs co-cultures reverted the negative effect

observed on the endothelial coverage in presence of CCs alone. This observation is supported by previous studies showing that platelets release pro-survival molecules and mitogens including bFGF and VEGF, which are both key regulators of EC survival and proliferation.[55]

Overall, these preliminary observations on CC and endothelial changes in presence of platelets, neutrophils or both prompted us to study the process of CC TEM in a 3D microenvironment including all the major components of the EMN. Our results show that platelets and neutrophils together influence the process of extravasation in the 3D EMN microenvironment by significantly increasing TEM compared to CCs alone.

Besides the investigation of key mechanisms involved in the EMN formation and evolution, our combination of *in vitro* models can be exploited to dissect the action of specific drugs within the niche. To demonstrate this potential application, we characterized the effects of eptifibatide, a clinically approved anti-aggregant drug which inhibits $\alpha_{IIb}\beta_3$ and $\alpha_v\beta_3$ integrins. These integrins are expressed by nearly all the components of the EMN. In particular, the β_3 subunit is associated to the α_{IIb} subunit in platelets[31] and to the α_v subunit in ECs.[46] $\alpha_{IIb}\beta_3$ is fundamental for platelet aggregation and subsequent activation and is also involved in CC TEM.[34] Recently, it has been shown that the integrin β_3 subunit is also expressed by breast CCs, either associated to α_{IIb}[56] or to α_v.[57] Importantly, the expression of this subunit has been shown to promote CC metastatic potential.[58] Here we observed a significant decrease of CC TEM when co-cultures of platelets, neutrophils and CCs were treated with eptifibatide and infused into the vascular network inside microfluidic devices. In addition, eptifibatide limited CC adhesion to microvascular networks and invasion of a 3D matrix when CCs were co-injected with platelets and neutrophils. These effects are due to concurrent mechanisms occurring in different components of the niche. Indeed, the addition of eptifibatide reduced the number of platelet and neutrophil aggregates, supporting a decrease in platelet activation. Furthermore, inhibition of integrin β_3 reduced morphological signatures of CC invasiveness (circularity data) and the expression of EMT and invasiveness markers, which are indicators of an aggressive phenotype. Previous studies showed that PAI-1, MMP-9 and other invasion markers including Snail and Vimentin are significantly upregulated upon co-culture of CCs with platelets,[10] but to our knowledge it has never been reported that inhibition of integrin β_3 could downregulate those markers in CCs co-cultured with platelets, neutrophils and ECs. The reduction of PAI-1 expression after treatment with eptifibatide was not observed in the absence of neutrophils in the co-culture system (ESI† Fig. S7). Although preliminary, this finding again suggests that neutrophils might have a role in limiting CC invasion.

We next tested the effect of β_3 inhibition on the expression and activation in CCs of proteins belonging to the focal adhesion complex, which mediates integrin-related signaling processes[59-61] and cytoskeleton remodeling during invasion.[62,63] The decreased expression and phosphorylation of TLN1 and FAK in treated CCs allows to suggest their involvement in the impaired invasive potential of CCs, as reported for other CC types.[64] Besides its effect on CCs, inhibition of β_3 in the co-culture system limited VE-cadherin[Y658] phosphorylation and its nuclear localization. Interestingly, VE-cadherin[Y658] phosphorylation and internalization towards the nucleus leads to junction disruption, which is required for CC extravasation. Previous findings[48] demonstrated the key role of Src and FAK activation in VE-cadherin[Y658] phosphorylation and in the determination of inter-endothelial junction architecture. Here, we additionally showed that Src-FAK-VE-cadherin signaling axis can be modulated by integrin β_3 inhibition. Furthermore, inhibition of β_3 integrin led to a significant decrease in vascular permeability, further contributing to the observed decrease in CC TEM.

In conclusion, our EMN-on-a-chip coupled with a multi-culture strategy allowed us to demonstrate for the first time the effects and the potential mechanisms of action of eptifibatide, whose application outside the field of blood disorders was previously unappreciated. The EMN-on-a-chip recapitulated the main components of its *in vivo* counterpart, proving that the integrin β_3 inhibitor eptifibatide could actually perform as an anti-metastatic agent. In parallel, the array of co-culture assays allowed us to dig into the mechanisms of action of the drug, providing evidence that eptifibatide goes beyond its traditional role of anti-aggregant drug, affecting both CC invasive ability and endothelium properties. We believe that the results obtained through our multi-culture strategy will pave the way for a better understanding of the promising applications of eptifibatide in the fields of cancer biology and vascular biology. In addition, we think that our approach can be employed to further investigate metastatic mechanisms and can be easily implemented for the identification of novel and previously neglected applications of other already clinically approved drugs.

Conflicts of interest

The authors declare no competing interests.

Acknowledgements

References

1 J. Massagué and A. C. Obenauf, *Nature*, 2016, 529, 298–306.

2   Z. Granot, E. Henke, E. A. Comen, T. A. King, L. Norton and R. Benezra, *Cancer Cell*, 2011, 20, 300‒314.

3   M. Labelle and R. O. Hynes, *Cancer Discovery*, 2012, 2, 1091‒1099.

4   B. Psaila and D. Lyden, *Nat. Rev. Cancer*, 2009, 9, 285‒293.

5   M. Labelle, S. Begum and R. O. Hynes, *Proc. Natl. Acad. Sci. U. S. A.*, 2014, 111, E3053‒E3061.

6   S. Vanharanta and J. Massague, *Cancer Cell*, 2013, 24, 410‒421.

7   X. R. Xu, G. M. Yousef and H. Ni, *Blood*, 2018, 131, 1777‒1789.

8   J. H. Im, W. Fu, H. Wang, S. K. Bhatia, D. A. Hammer, M. A. Kowalska and R. J. Muschel, *Cancer Res.*, 2004, 64, 8613‒8619.

9   B. Nieswandt, M. Hafner, B. Echtenacher and D. N. Männel, *Cancer Res.*, 1999, 59, 1295‒1300.

10 M. Labelle, S. Begum and R. O. Hynes, *Cancer Cell*, 2011, 20, 576‒590.

11 L. J. Gay and B. Felding-Habermann, *Nat. Rev. Cancer*, 2011, 11, 123‒134.

12 D. Schumacher, B. Strilic, K. K. Sivaraj, N. Wettschureck and S. Offermanns, *Cancer Cell*, 2013, 24, 130‒137.

13 S. Massberg, I. Konrad, K. Schürzinger, M. Lorenz, S. Schneider, D. Zohlnhoefer, K. Hoppe, M. Schiemann, E. Kennerknecht, S. Sauer, C. Schulz, S. Kerstan, M. Rudelius, S. Seidl, F. Sorge, H. Langer, M. Peluso, P. Goyal, D. Vestweber, N. R. Emambokus, D. H. Busch, J. Frampton and M. Gawaz, *J. Exp. Med.*, 2006, 203, 1221‒1233.

14 S. Karpatkin and E. Pearlstein, *Ann. Intern. Med.*, 1981, 95, 636‒641.

15 Z. G. Fridlender, J. Sun, S. Kim, V. Kapoor, G. Cheng, L. Ling, G. S. Worthen and S. M. Albelda, *Cancer Cell*, 2009, 16, 183‒194.

16 T. Kitamura, B. Z. Qian, D. Soong, L. Cassetta, R. Noy, G. Sugano, Y. Kato, J. Li and J. W. Pollard, *J. Exp. Med.*, 2015, 212, 1043‒1059.

17 S. J. Huh, S. Liang, A. Sharma, C. Dong and G. P. Robertson, *Cancer Res.*, 2010, 70, 6071‒6082.

18 M. J. Slattery and C. Dong, *Int. J. Cancer*, 2003, 106, 713‒722.

19 J. D. Spicer, B. McDonald, J. J. Cools-Lartigue, S. C. Chow, B. Giannias, P. Kubes and L. E. Ferri, *Cancer Res.*, 2012, 72, 3919‒3927.

20 S. K. Wculek and I. Malanchi, *Nature*, 2015, 528, 413‒417.

21 M. Saini, B. M. Szczerba and N. Aceto, *Cancer Res.*, 2019, 79, 6067‒6073.

22 M. B. Chen, C. Hajal, D. C. Benjamin, C. Yu, H. Azizgolshani, R. O. Hynes and R. D. Kamm, *Proc. Natl. Acad. Sci. U. S. A.*, 2018, 115, 7022‒7027.

23 W. Liang and N. Ferrara, *Cancer Immunol. Res.*, 2016, 4, 83‒91.

24 M. Gershkovitz, T. Fainsod-Levi, S. Khawaled, M. E. Shaul, R. V. Sionov, L. Cohen-Daniel, R. I. Aqeilan, Y. D. Shaul, Z. G. Fridlender and Z. Granot, *Cancer Res.*, 2018, 78, 5050‒5059.

25 N. C. Walsh, L. L. Kenney, S. Jangalwe, K. E. Aryee, D. L. Greiner, M. A. Brehm and L. D. Shultz, *Annu. Rev. Pathol.: Mech. Dis.*, 2017, 12, 187‒215.

26 H. C. Chen, *Methods Mol. Biol.*, 2005, 294, 15‒22.

27 S. N. Bhatia and D. E. Ingber, *Nat. Biotechnol.*, 2014, 32, 760‒772.

28 S. Bersini, C. Arrigoni, S. Lopa, M. Bongio, I. Martin and M. Moretti, *Drug Discovery Today*, 2016, 21(9), 1429‒1436.

29 P. H. McMinn, L. E. Hind, A. Huttenlocher and D. J. Beebe, *Lab Chip*, 2019, 19, 3697‒3705.

30 B. Saha, T. Mathur, K. F. Handley, W. Hu, V. Afshar-Kharghan, A. K. Sood and A. Jain, *Blood Adv.*, 2020, 4, 3329‒3342.

31 Y. J. Shimada, S. Bansilal, S. D. Wiviott, R. C. Becker, R. A. Harrington, A. Himmelmann, B. Neely, S. Husted, S. K. James, H. A. Katus, R. D. Lopes, P. G. Steg, R. F. Storey, L. Wallentin and C. P. Cannon, *Am. Heart J.*, 2016, 177, 1‒8.

32 A. Elbadawi, G. Gasioch, I. Y. Elgendy, A. N. Mahmoud, L. D. Ha, H. Al Ashry, H. Shahin, M. A. Hamza, A. S. Abuzaid and M. Saad, *Cardiol. Ther.*, 2016, 5, 203‒213.

33 A. Boucharaba, C.-M. Serre, S. Grès, J. S. Saulnier-Blache, J.-C. Bordet, J. Guglielmi, P. Clézardin and O. Peyruchaud, *J. Clin. Invest.*, 2004, 114, 1714‒1725.

34 F. Zhao, L. Li, L. Guan, H. Yang, C. Wu and Y. Liu, *Cancer Lett.*, 2014, 344, 62‒73.

35 M. Haemmerle, R. L. Stone, D. G. Menter, V. Afshar-Kharghan and A. K. Sood, *Cancer Cell*, 2018, 33(6), 965‒983.

36 A. Amirkhosravi, S. A. Mousa, M. Amaya, S. Blaydes, H. Desai, T. Meyer and J. L. Francis, *Thromb. Haemostasis*, 2003, 90, 549‒554.

37 J. S. Jeon, S. Bersini, M. Gilardi, G. Dubini, J. L. Charest, M. Moretti and R. D. Kamm, *Proc. Natl. Acad. Sci. U. S. A.*, 2015, 112, 214‒219.

38 M. B. Chen, J. A. Whisler, J. Fröse, C. Yu, Y. Shin and R. D. Kamm, *Nat. Protoc.*, 2017, 12, 865‒880.

39 J. S. Jeon, S. Bersini, J. A. Whisler, M. B. Chen, G. Dubini, J. L. Charest, M. Moretti and R. D. Kamm, *Integr. Biol.*, 2014, 6, 555‒563.

40 E. T. Roussos, J. S. Condeelis and A. Patsialou, *Nat. Rev. Cancer*, 2011, 11, 573‒587.

41 J. Villagra, S. Shiva, L. A. Hunter, R. F. Machado, M. T. Gladwin and G. J. Kato, *Blood*, 2007, 110, 2166‒2172.

42 E. Bousquet, O. Calvayrac, J. Mazières, I. Lajoie-Mazenc, N. Boubekeur, G. Favre and A. Pradines, *Oncogene*, 2016, 35, 1760‒1769.

43 T. Shibue, M. W. Brooks and R. A. Weinberg, *Cancer Cell*, 2013, 24, 481‒498.

44 P. Ghiabi, J. Jiang, J. Pasquier, M. Maleki, N. Abu-Kaoud, S. Rafii and A. Rafii, *PLoS One*, 2014, 9(11), e112424.

45 L. S. Steelman, W. H. Chappell, S. L. Abrams, C. R. Kempf, J. Long, P. Laidler, S. Mijatovic, D. Maksimovic-Ivanic, F. Stivala, M. C. Mazzarino, M. Donia, P. Fagone, G. Malaponte, F. Nicoletti, M. Libra, M. Milella, A. Tafuri, A. Bonati, J. Bäsecke, L. Cocco, C. Evangelisti, A. M. Martelli, G. Montalto, M. Cervello and J. A. McCubrey, *Aging*, 2011, 3, 192‒222.

46 S. J. Atkinson, T. S. Ellison, V. Steri, E. Gould and S. D. Robinson, *Biochem. Soc. Trans.*, 2014, 42, 1590‒1595.

47 D. Cox, M. Brennan and N. Moran, *Nat. Rev. Drug Discovery*, 2010, 9, 804–820.

48 C. Jean, X. L. Chen, J. O. Nam, I. Tancioni, S. Uryu, C. Lawson, K. K. Ward, C. T. Walsh, N. L. Miller, M. Ghassemian, P. Turowski, E. Dejana, S. Weis, D. A. Cheresh and D. D. Schlaepfer, *J. Cell Biol.*, 2014, 204, 247–263.

49 B. M. Szczerba, F. Castro-Giner, M. Vetter, I. Krol, S. Gkountela, J. Landin, M. C. Scheidmann, C. Donato, R. Scherrer, J. Singer, C. Beisel, C. Kurzeder, V. Heinzelmann-Schwarz, C. Rochlitz, W. P. Weber, N. Beerenwinkel and N. Aceto, *Nature*, 2019, 566, 553–557.

50 H. B. Acuff, K. J. Carter, B. Fingleton, D. L. Gorden and L. M. Matrisian, *Cancer Res.*, 2006, 66, 259–266.

51 S. Valastyan and R. A. Weinberg, *Cell*, 2011, 147, 275–292.

52 C. M. Ghajar, H. Peinado, H. Mori, I. R. Matei, K. J. Evason, H. Brazier, D. Almeida, A. Koller, K. A. Hajjar, D. Y. R. Stainier, E. I. Chen, D. Lyden and M. J. Bissell, *Nat. Cell Biol.*, 2013, 15, 807–817.

53 R. T. P. Poon, C. P. Y. Lau, S. T. Cheung, W. C. Yu and S. T. Fan, *Cancer Res.*, 2003, 63, 3121–3126.

54 M. D. Potter, S. Barbero and D. A. Cheresh, *J. Biol. Chem.*, 2005, 280, 31906–31912.

55 G. Pintucci, S. Froum, J. Pinnell, P. Mignatti, S. Rafii and D. Green, *Thromb. Haemostasis*, 2002, 88, 834–842.

56 J. Kononczuk, A. Surazynski, U. Czyzewska, I. Prokop, M. Tomczyk, J. Palka and W. Miltyk, *Curr. Drug Targets*, 2015, 16, 1429–1437.

57 M. H. Ross, A. K. Esser, G. C. Fox, A. H. Schmieder, X. Yang, G. Hu, D. Pan, X. Su, Y. Xu, D. V. Novack, T. Walsh, G. A. Colditz, G. H. Lukaszewicz, E. Cordell, J. Novack, J. A. J. Fitzpatrick, D. L. Waning, K. S. Mohammad, T. A. Guise, G. M. Lanza and K. N. Weilbaecher, *Cancer Res.*, 2017, 77, 6299–6312.

58 K. A. Kwakwa and J. A. Sterling, *Cancers*, 2017, 9.

59 D. A. Calderwood, V. Tai, G. Di Paolo, P. De Camilli and M. H. Ginsberg, *J. Biol. Chem.*, 2004, 279, 28889–28895.

60 D. R. Critchley and A. R. Gingras, *J. Cell Sci.*, 2008, 121, 1345–1347.

61 A. Desiniotis and N. Kyprianou, in *International Review of Cell and Molecular Biology*, Elsevier Inc., 2011, vol. 289, pp. 117–147.

62 J. K. Jin, P. C. Tien, C. J. Cheng, J. H. Song, C. Huang, S. H. Lin and G. E. Gallick, *Oncogene*, 2014, 34, 1811–1821.

63 B. Tavora, L. E. Reynolds, S. Batista, F. Demircioglu, I. Fernandez, T. Lechertier, D. M. Lees, P. P. Wong, A. Alexopoulou, G. Elia, A. Clear, A. Ledoux, J. Hunter, N. Perkins, J. G. Gribben and K. M. Hodivala-Dilke, *Nature*, 2015, 514, 112–116.

64 P. P. Shah, M. Y. Fong and S. S. Kakar, *Oncogene*, 2012, 31, 3124–3135.